

IMPROVED TOTAL VARIATION-TYPE REGULARIZATION USING HIGHER-ORDER EDGE DETECTORS

W. STEFAN* R. RENAUT† AND A. GELB‡

Abstract. We present a novel deconvolution approach to accurately restore piecewise smooth signals from blurred data. The first stage uses *Higher Order* Total Variation restorations to obtain an estimate of the location of jump discontinuities from the blurred data. In the second stage the estimated jump locations are used to determine the local orders of a *Variable Order* Total Variation restoration. The method replaces the first order derivative approximation used in standard Total Variation by a variable order derivative operator. Smooth segments as well as jump discontinuities are restored while the *staircase effect* typical for standard first order Total Variation regularization is avoided. As compared to first order Total Variation, signal restorations are more accurate representations of the true signal, as measured in a relative l^2 norm. The method can also be used to obtain an accurate estimation of the locations and sizes of the true jump discontinuities. The approach is independent of the algorithm used for the standard Total Variation problem and is, consequently, readily incorporated in existing Total Variation restoration codes.

1. Introduction. The accurate identification and quantification of physical structures in signals, from small to large scales, presents a number of challenges which are dependent on the data acquisition and reconstruction architectures. Whereas an underlying signal of interest may contain jump discontinuities, its recorded or reconstructed data is usually contaminated by both blur and noise¹. In restoring the original signal it is important to retain or determine its original properties. The edges and inherently smooth regions should be preserved, while the jump discontinuities that separate smooth regions should be identified.

Signal deblurring and edge detection are typically addressed independently. For example, in standard image deblurring for given recorded data and a known Point Spread Function (PSF), or blurring kernel, restoration of the signal subject to First Order Total Variation (FOTV) regularization leads to preservation of the edges [5, 18, 13, 25]. But because the method relies on the assumption that the underlying signal consists of piecewise constant components, the restored signal also exhibits many false jump discontinuities (edges); the so-called *staircase effect*. On the other hand, high accuracy detection of edges in unblurred signals has been addressed separately, e.g. by the polynomial annihilation edge detection method in [1] or by renormalized local (undivided) differences in [8]. Through the combination of both edge detection and Total Variation (TV) regularized deconvolution, we seek to eliminate the staircase effect while also accurately detecting **true** jump discontinuities.

The main idea of our new approach is to replace the linear first order derivative operator used in FOTV by a linear variable order difference operator. The variable order difference operator applies different order undivided differences to the signal depending on the locations of jump discontinuities. The resulting numerical optimization problem can be solved using standard numerical methods. There are two separate stages, in the first stage jump discontinuity locations are estimated using multiple Higher Order Total Variation (HOTV) restorations of the blurred signal. Restorations, which are piecewise polynomials, are combined using the **minmod** limiter [14, 8]². In the second stage, the estimate of the locations of the edges is used to select the order for a Variable Order Total Variation (VOTV) regularized deconvolution. The resulting deblurring algorithm better preserves the smooth regions of a restored signal as compared to the standard FOTV regularized deconvolution, and also provides a much better approximation of the jump function of the signal. Numerical experiments demonstrate the performance of the method for different PSFs which determine the kind and degree of blurring in the signal. We do not add any noise, however, other than noise resulting from using finite precision arithmetic.

The paper is structured as follows: FOTV regularization is reviewed in Section 2.1 and important

*ARIZONA STATE UNIVERSITY, DEPARTMENT OF MATHEMATICS AND STATISTICS, TEMPE, AZ 85287-1804. TEL: 480-965-0401. EMAIL WOLFGANG.STEFAN@ASU.EDU

†ARIZONA STATE UNIVERSITY, DEPARTMENT OF MATHEMATICS AND STATISTICS, TEMPE, AZ 85287-1804. TEL: 480-965-3795, FAX: 480-965-4160. EMAIL: RENAUT@ASU.EDU

‡ARIZONA STATE UNIVERSITY, DEPARTMENT OF MATHEMATICS AND STATISTICS, TEMPE, AZ 85287-1804. TEL: 480-965-3793/0559, FAX: 480-965-8119. EMAIL: AG@ASU.EDU

¹Here we only consider noise resulting from using finite precision arithmetic.

²Originally used for oscillation reduction in the numerical solutions of Partial Differential Equations, e.g in [14], and later used to reduce oscillations of higher order edge detectors in [8].

relevant results from [8] and [1] that lead to development of linear variable-order local difference operators used for edge detection are summarized in Section 2.2. These variable-order difference operators are used for regularized deconvolution in Section 3. Performance of the algorithm for various blurs and with respect to different parameters is discussed in Section 3.3. We conclude, in Section 4, that the method provides a novel approach for simultaneously handling edge detection and deblurring. It will therefore lead to improved feature extraction from blurred signals.

2. Signal Restoration and Edge Detection.

2.1. First Order Total Variation. We suppose that the given signal $g = f * h + n$ is a blurred and noisy version of the unknown true signal f , where $*$ is the convolution operator, h is the Spatially Invariant Point Spread Function (SIPSF) which describes the blurring of f , and n is noise. The convolution operator can be defined for periodic, zero, or constant boundary conditions. Here we assume, without loss of generality, periodic boundaries. An approximation to f can be obtained as a solution of the variational problem, for example see [13, 25],

$$\min_{\hat{f}} \left\{ \mathbf{Fid}_h(\hat{f}, g) + \lambda \mathbf{Reg}(\hat{f}) \right\}. \quad (2.1)$$

$\mathbf{Fid}_h(\hat{f}, g)$ is the data-fidelity, or fit-to-data, term which measures how well \hat{f} fits signal g for given PSF h , here estimated using the Least Squares (LS) fit,

$$\mathbf{Fid}_h(\hat{f}, g) = \|\hat{f} * h - g\|_2^2. \quad (2.2)$$

The regularization term $\mathbf{Reg}(\hat{f})$ serves to penalize high noise solutions and to restrict the solution space to the desired class of functions, e.g. piecewise constant or piecewise smooth. A popular choice uses the semi-norm

$$\mathbf{Reg}(\hat{f}) = TV(\hat{f}) = \|L\hat{f}\|_1, \quad (2.3)$$

where L is a discrete differentiation operator, usually a first-order Finite Difference (FD) approximation of the first derivative [25, 13, 9]. The choice of the regularization parameter λ , which depends on the noise level and governs how much regularization will be applied, is not a focus of this paper, but is in general an active field of research, e.g. [15, 16, 20, 21].

The variational problem (2.1) using (2.2) and (2.3) is a convex optimization problem and can be solved by a number of algorithms. In the stated form (2.1) it can be solved by e.g. the continuation method in [26], or by quasi-Newton methods if (2.3) is replaced by

$$\mathbf{Reg}(\hat{f}, \beta) = \sum_i \sqrt{(L\hat{f})_i^2 + \beta^2}, \quad (2.4)$$

with small $\beta > 0$. Alternatively (2.1) can be reformulated as a Second Order Cone Program (SOCP):

$$\min_{\mathbf{w}} \sum_{i=1}^n \mathbf{w}_i \quad \text{subject to} \quad \begin{cases} \mathbf{Fid}(\hat{f}, g) \leq \sigma \\ |(L\hat{f})_i| \leq \mathbf{w}_i \end{cases}, \quad (2.5)$$

where the bound constraint on $L\hat{f}$ is the so called *cone condition* and σ is related to λ by the Karush-Kuhn-Tucker (KKT) condition (see [17, Chapter 12]). Barrier function methods or dual interior point methods [11, 12, 23, 24] can be used to solve (2.5). The results in this paper, however, do not depend on the chosen method.

It is well known that minimization with respect to the \mathcal{L}^1 norm yields a sparse solution [3, 4]. For the \mathcal{L}^1 norm of the FOTV, therefore, the derivative of the solution will be zero except at isolated points. In particular, the solution itself will be piecewise constant and smooth regions will be approximated by a staircase function. Equivalently, (2.3) is only a good choice if the signal to be restored is piecewise constant.

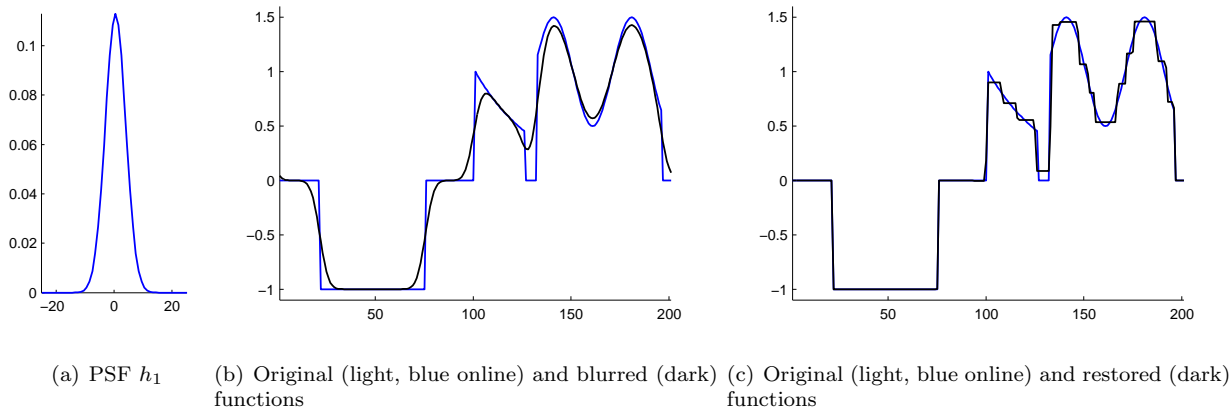


FIG. 2.1. In (b) the piecewise smooth test function is contaminated by blurring with the Gaussian of 9 pixels Full Width at Half Maximum (FWHM), illustrated in (a). Panel (c) shows the result of the FOTV restoration with $\lambda = 10^{-3}$, which yields an l^2 error of .083. The edges are mostly preserved but the smooth regions are approximated by the typical piecewise constant staircases.

This is illustrated in Figure 2.1, in which the restored signal, obtained from the blurred piecewise smooth test function, exhibits the false jump discontinuities that result from the staircase effect of the FOTV regularization.

In order to reduce the staircase effect we propose to find an alternative operator L to use in the regularization such that the resulting restorations still maintain the property of sparseness for piecewise smooth signals, while also correctly identifying jump locations. In particular we replace the operator L in (2.3) by an approximation of the jump function, defined in Section 2.2, such that Lf is sparse for piecewise smooth functions. In the next section we review the method in [8] used to approximate jump functions for functional data only given on discrete grid points.

2.2. Local detection of edges using local (undivided) differences. The jump function of a piecewise smooth $f(x)$ is defined by

$$[f](x) = f(x^+) - f(x^-), \quad (2.6)$$

where x^+ and x^- are the well defined right and left hand limits at a point x , respectively. It is identically zero, $[f](x) = 0$, on intervals where f is smooth. Scaled local difference operators as described in [1, 8] are linear translation-invariant operators approximating $[f](x)$, for functions defined on a discrete grid that effectively separate jump discontinuities of $f(x)$ from regions where $f(x)$ is smooth.

It suffices for our deconvolution application to assume that $f(x)$ is sampled at equally spaced points with spacing Δx . Suppose that $S_x := \{x_1, \dots, x_{m+1}\}$ is an ordered stencil, $x_j = x_{j-1} + \Delta x$, such that $x_1 < x < x_{m+1}$. The local difference operator of order m at x is defined by

$$\Delta_{S_x}^m f(x) = \sum_{x_k \in S_x} c_{m,k} f(x_k), \quad (2.7)$$

where the coefficients $c_{m,k}$ are given by

$$c_{m,k} = -\frac{m!}{\prod_{j=1, j \neq k}^{m+1} (k-j)}, \quad (2.8)$$

and only depend on the size of the stencil but not on the reconstruction point³ x . These operators, normalized to appropriate size, are shown to converge to the jump function (2.6) with order m away from the jumps

³The coefficients $c_{m,k}$ depend on x in case non-equally spaced points are used, see [1].

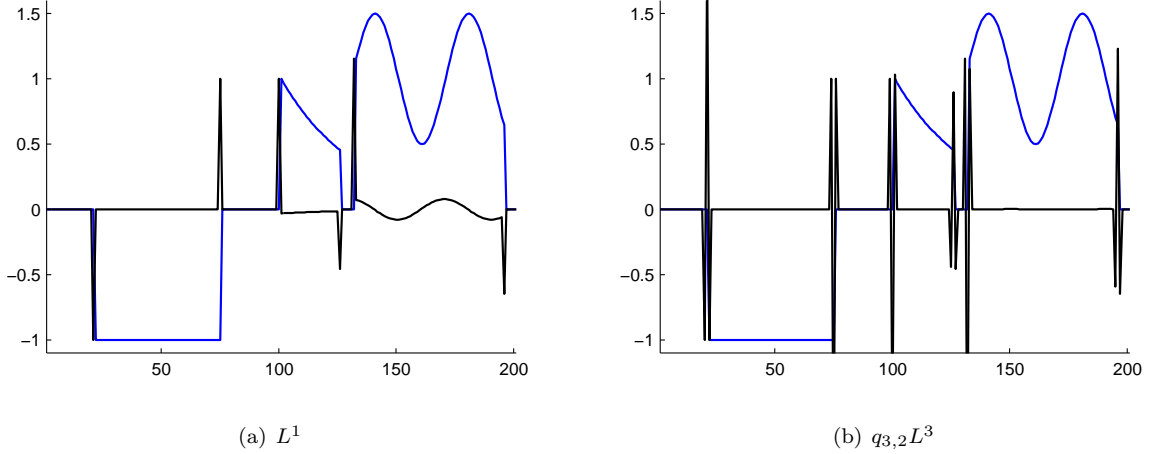


FIG. 2.2. Jump function estimates for a test function (light, blue online) with several jump discontinuities and different gradients in the smooth regions. The low order method, L^1 , panel (a), has no oscillations around the edges but is non-zero in the smooth regions with non-zero gradient. The higher-order method, L^3 , scaled to preserve the height of the jump by $q_{3,2} = 1/2$, panel (b), has oscillations around the jump discontinuities but is almost zero in the smooth regions.

The true jump function is

$$[\mathbf{h}](x_{j+1/2}) = \begin{cases} 0 & \text{for } j < 0 \text{ and } j > 0 \\ 1 & \text{for } j = 0 \end{cases},$$

and in approximating $[\mathbf{h}](x_{-1/2})$ using $q_{1,1}L^1$ and $q_{3,2}L^3$, it is easy to see that L^1 correctly gives 0 while L^3 does not because the convolution kernel crosses over the jump discontinuity, i.e. its support is too large. A general discussion on the convergence of edge detectors based on local difference operators can be found in [8].

2.3. The minmod limiter and a variable order edge detector. To overcome the problem of oscillations around the jump discontinuity the **minmod** limiter can be applied to the jump function approximations $q_{m,i}L_i^m f$ [8]. The idea is to compare results for different orders at a particular point x and define

$$(L^{\text{minmod}} f)_j = \mathbf{minmod}\{(q_{m,i}L_i^m f)_j, \text{ for all pairs } (m, i)\}, \quad (2.13)$$

with

$$\mathbf{minmod}\{a_1, a_2, \dots, a_n\} := \begin{cases} s \cdot \min(|a_1|, |a_2|, \dots, |a_n|) & \text{if } \text{sgn}(a_1) = \dots = \text{sgn}(a_n) := s \\ 0 & \text{otherwise} \end{cases}, \quad (2.14)$$

where $q_{m,i}$ are chosen such that the height of the jump is preserved, see [1].

Most of the oscillations in the neighborhood of a jump are eliminated, as is demonstrated in Figure 2.3(a), for the **minmod** limiter taken over all stencils up to order $m = 5$. On the other hand, due to its inherent nonlinearity the **minmod** operation is not well suited for incorporation as a regularization term in the deconvolution and an alternative formulation is needed.

Assuming the locations of the jump discontinuities are known, or can be estimated for example by the **minmod** limiter in a reprocessing phase, the formation of oscillations around the jump discontinuities can also be avoided by using an x -dependent order $m(x)$. By choosing $m = 1$ at the jump discontinuities and increasing the order away from the jump discontinuities, the advantages of higher-order methods can be exploited without the formation of oscillations around the jump discontinuities. The stencil around the restoration point is chosen such that it does not overlap with the jump discontinuities and is of order

$m(x_{j+1/2}) = \frac{d(x_{j+1/2})}{\Delta x} + 1$, where

$$d(x) = \min\{|x - y| | y \in J\}, \quad (2.15)$$

and $J = \{x : [f](x) \neq 0\}$. For example, a portion of a variable order local difference operator $L_{i(x)}^{m(x)}$ might be

$$L_{i(x)}^{m(x)} = \begin{bmatrix} & & & & \vdots & & & & \\ & & & & & & & & \\ & & 1 & -3 & 3 & -1 & & & \\ & & & -1 & 2 & -1 & & & \\ \dots & & & & & 1 & -1 & & \dots \\ & & & & & & -1 & 2 & -1 \\ & & & & & & -1 & 3 & -3 & 1 \\ & & & & & & \vdots & & & \end{bmatrix}, \quad (2.16)$$

where $i(x)$ is chosen such that stencils of order $m > 1$ do not cross jump discontinuities and we drop $i(x)$ for the rest of this paper. The resulting jump detector $L^{m(x)}$ is now a convolution operator with a Spatially Variant Point Spread Function (SVPSF), whose values are computed by (2.8). It converges to the jump function (2.6) as $N \rightarrow \infty$ only for the class of functions that have jump discontinuities at $x \in J$. Unlike **minmod** alone, the edge detector $L^{m(x)}$ is a linear operator which ensures that (2.3) remains convex and can be formulated as a SOCP when L is replaced by $L^{m(x)}$ in the regularization term of the deconvolution. The result of using the SVPSF edge detector is shown in Figure 2.3(b), which illustrates the use of the variable-order edge detector with increasing order away from the jump discontinuities up to order $m = 5$, and demonstrates that the oscillations around the jump discontinuities are avoided.

Algorithm 1 summarizes the procedure for the construction of a variable-order edge detector for uncontaminated signals.

Algorithm 1

(* linear higher-order edge detectors *)

1. Given piecewise smooth function sampled on regular grid $f_j := f(x_j)$, $x_j \in S$, order m and threshold θ
2. Compute jump function approximation $L^{\text{minmod}} f$ by (2.13)
3. Compute SVPSF edge detector matrix $L^{m(x)}$ using jump locations given by $J = \{x_{j+1/2} : |(L^{\text{minmod}} f)_j| > \theta\}$.

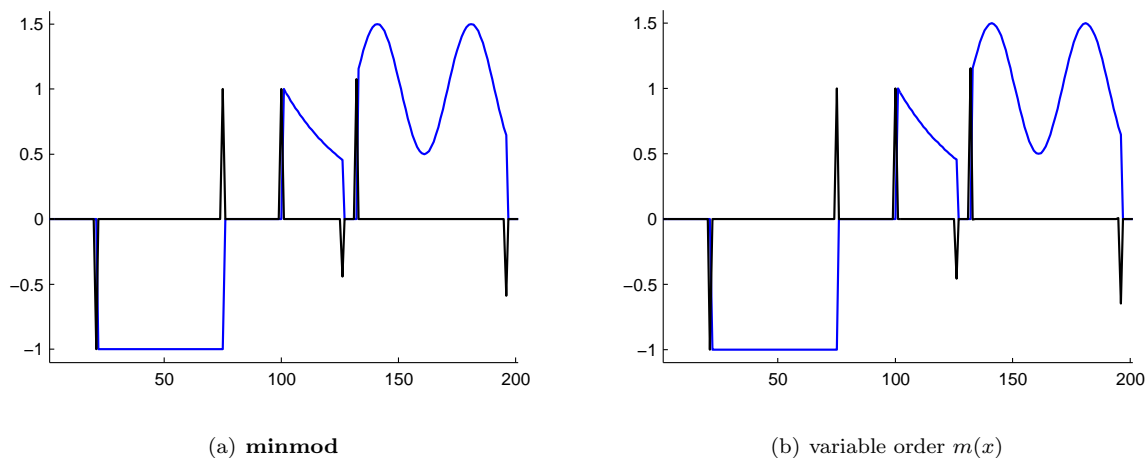


FIG. 2.3. The **minmod** method and the variable-order method are both able to greatly reduce the oscillations around the jump discontinuities, as compared to the examples illustrated in Figure 2.2.

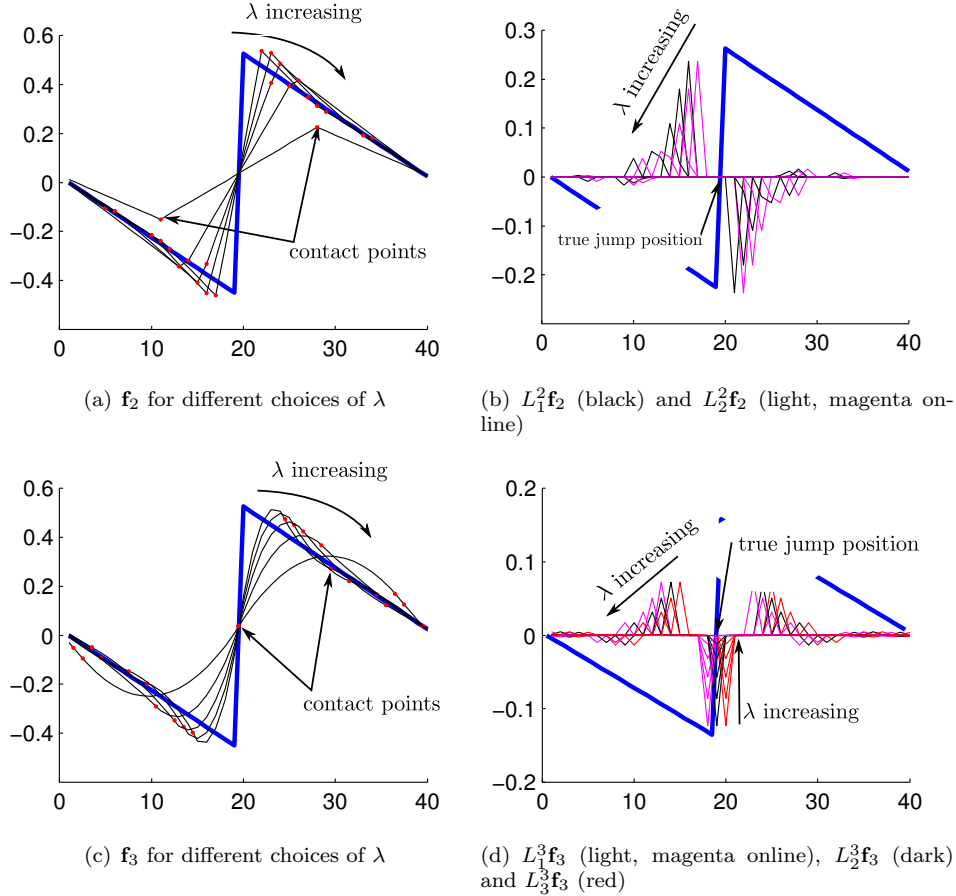


FIG. 3.1. Different stencils are used to restore the test function (light, blue online) in (a) and (c). Panel (a) shows the second order restoration. The contact points between the polynomial segments (light dots, red dots online) move away from the jump location with increasing λ . The jump function approximation in panel (b) also illustrates this behaviour. Panel (c) shows a third order restoration for increasing λ . Panel (d) shows the jump function approximation using different third order stencils: L_1^3 (light, magenta online), $L_2^3 = L^3$ (dark), L_3^3 (light, red online). These figures suggests that, of those illustrated here, the correct jump location is only provided by $L_2^3 = L^3$.

3. Signal deconvolution using regularization with higher-order TV. Equipped with a linear SVPSF, and prior knowledge of the edge locations in the signal, the FOTV operator $L = L^1$ in the regularization term can be replaced by the scaled variable-order edge detector $L^{m(x)}$ as

$$\mathbf{Reg}(\hat{f}) = \|\text{diag}(C_{m(x)})L^{m(x)}\hat{f}\|_1, \quad (3.1)$$

where we allow an order dependent scaling by constants $C_1, \dots, C_{m_{\max}}$ which we will specify later. Note that if $\text{diag}(C_{m(x)})L^{m(x)}$ is used for edge detection, then $C_1 = 1$ ensures that $(\text{diag}(C_{m(x)})L^{m(x)})f$ converges to $[f](x)$ as $N \rightarrow \infty$. The cost functional (2.1) using the linear operator (3.1) is still a SOCP and can be solved as before using standard SOCP solvers.

3.1. Edge location detection in blurred data using HOTV restorations. Generally there is no a priori knowledge of the edge locations but L can be replaced by any local difference operator L_i^m , thus maintaining the use of the SOCP algorithm and resulting in HOTV regularization.

NOTE 1. The discrete restoration $\mathbf{f}_m \in \mathbb{R}^N$ obtained using L_i^m in (2.5) or (2.1) is independent of i due to the shift invariance of $\|\cdot\|_1$ and is asymptotically, as $N \rightarrow \infty$, a piecewise polynomial of degree $m - 1$, with $m - 2$ continuous derivatives if $m > 1$, and jump discontinuities in the derivative of order $m - 1$. The derivative of order m of \mathbf{f}_m is only defined as a distribution with bounded \mathcal{L}^1 -norm and can be expressed as a

weighted sum of delta distributions centered at the locations of the contact points of the polynomial segments. The locations of the contact points are dynamically determined by the minimization of (2.1) and are thus dependent on λ . Larger λ result in smaller \mathcal{L}^1 norms of the m^{th} derivative with fewer delta distributions composing $f_m^{(m)}(x)$. For a finite grid $(L_i^m \mathbf{f}_m)_j \neq 0$ for $j \in J$ with $\#J \ll N$, where $\#J$ is the cardinality of the set J .

EXAMPLE 1. $m = 1$ (FOTV): FOTV restorations are piecewise constant with sparse derivatives while jump discontinuities in the original signal are preserved, i.e. there is a contact point of the piecewise constant segments at the location of the jump for small enough λ [22]. The locations of other contact points depend on the choice of λ .

EXAMPLE 2. $m = 2$ (second order TV): Consider the function in Figure 3.2 (a) which is approximated by piecewise polynomials of degree 1 that minimize (2.1) with $L = L_1^2$. The restoration \mathbf{f}_2 has a sparse second derivative, which satisfies $\|f_2^{(2)}\|_1 < \infty$, thus \mathbf{f}_2 is continuous with a piecewise constant first derivative. The jump in the original signal is approximated by a line crossing the jump discontinuity, as illustrated in Figure 3.1 (a) for different values of λ . The locations of the contact points between the line segments move away from the jump location with increasing λ because sharper angles between the line segments result in a larger regularization term in (2.1). Figure 3.1 (b) shows $L_1^2 \mathbf{f}_2$ and $L_2^2 \mathbf{f}_2$ which result from the two possible stencils for $m = 2$. Both L_1^2 and L_2^2 identify the non-zero second derivative that is expected from the asymptotic solution described in Note 1. Because the solution is computed on grid points the location of the jump discontinuity is only identified up to an one pixel shift which results from the shift in the stencil between L_1^2 and L_2^2 .

EXAMPLE 3. $m = 3$ (third order TV): Now consider the test function which is approximated by piecewise polynomials of degree 2, for which the jump is best approximated by two parabola branches connected at the location of the jump, see Figure 3.1 (c). The three possible stencils for L_i^3 , $i = 1, 2, 3$, identify the non-zero 3^{rd} derivative, expected from the asymptotic solution described in Note 1, again up to the shift in the stencil.

The examples above show that the locations of the contact points can be used to identify the locations of the jump discontinuities in the signal, for both $m = 1$ and $m = 3$ but not $m = 2$. In Appendix A we formulate the problem of approximating a step function with polynomial segments. The solutions suggest that even order polynomial approximations have minimal \mathcal{L}^2 -norm if the contact point of the piecewise polynomial segments is placed at the position of the step. We conclude that we can utilize the locations of contact points of odd order restorations \mathbf{f}_m using an approximation of $\mathbf{f}_m^{(m)}$ with centered stencils to estimate jump locations.

Methods for detecting jump discontinuities in $f^{(m-1)}$ for functions that are $C^{(m-2)}$ are presented in [2] and [19]. The restorations \mathbf{f}_m are, however, only approximations of piecewise polynomials and thus contain numerical noise and approximation errors. In order to avoid numerical instabilities when using such methods we use (2.12) and observe that $L^m \mathbf{f}_m$ are sparse by design and are, therefore, well suited to detect jump discontinuities in $\mathbf{f}_m^{(m-1)}$.

This procedure also results in false positives at contact points away from jump discontinuities. These can be reduced by applying the **minmod** limiter over the locations of the contact points of odd order restorations. Using the estimated locations of the jump discontinuities a variable order derivative $L^{m(x)}$ is constructed and used as regularization term (3.1) in a VOTV regularization. The process is described in Algorithm 2.

The use of HOTV regularization is illustrated for the signal (light, blue online) with jump located between grid points 19 and 20 in Figure 3.2(a). The blurred (dark) signal is obtained by blurring with the PSF h given in Figure 2.1(a). Example solutions \mathbf{f}_m , for $m = 1, 2, 3$ and 5 and their m^{th} local difference operator using $L_i^m \mathbf{f}_m$, are shown in panels (b)-(f), respectively, in which in each case the dashed (light, red online) line is the restored signal and the bold line is the m^{th} order local difference operator. Solution $L^1 \mathbf{f}_1$ shows several false positive jump locations close to and away from the jump due to the TV staircase effect. The second order solution \mathbf{f}_2 , panels (c) and (d), is piecewise linear and the two second order local difference operators, $L_1^2 \mathbf{f}_2$ and $L_2^2 \mathbf{f}_2$, do not correctly show the jump between points 19 and 20. On the other hand, the unbiased stencils, panels (e) and (f), correctly identify the location of the jump and the false positives are decreasing in size away from the true jump.

3.2. Signal restoration using VOTV. We can observe that the nonzero values of $L_i^m \mathbf{f}_m$ become smaller with increasing m . We use C_m in Algorithm 2 to compensate for this behaviour. In addition C_m determines how much *regularization* is applied with respect to the order m by L_m and $L_{m(x)}$. Alternatively we can consider an order dependent regularization parameter $\lambda(m)$, where $\lambda(m) = C_m \lambda(1)$. From the Taylor expansion of smooth signals we can expect to obtain reasonable results for $C_m = m!$, but C_m also has an impact on the ability of L_m to penalize noise in non-smooth solutions. Because choosing such regularization parameters is still an open question we choose $C_m = m!$ empirically which should lead to similar λ for all m .

The **minmod** approximation of the jump function over all odd order unbiased stencils up to order $m_{\max} = 5$, i.e. using L^1, L^3, L^5 for L in (2.5), is shown in panel (g) and the resulting approximation of f obtained using the SVPSF $L^{m(x)}$ in panel (h). The restoration has a relative l^2 error of 0.0052 as compared to 0.1511 of the FOTV solution, but is of course still dependent on the choice of λ .

Algorithm 2

(* Regularization using linear higher-order edge detectors *)

1. Given a piecewise smooth blurred function sampled on a regular grid $g_j := g(x_j)$, parameter λ , odd maximal order m_{\max} , threshold θ and weights $C_1, \dots, C_{m_{\max}}$
2. Compute matrices $L^1, L^3, L^5, \dots, L^{m_{\max}}$ using (2.7)
3. Restore FOTV approximation \mathbf{f}_1 using L^1 in (2.1) and calculate residual $\sigma = \mathbf{Fid}_h(\mathbf{f}_1, g)$
4. Restore HOTV approximations \mathbf{f}_m using (2.5) with L^m for L
5. Compute normalized **minmod** approximation of the common contact points $\bar{f} = c \cdot \mathbf{minmod}\{|L^m \mathbf{f}_m|, \forall m\}$, with c chosen such that $\max_x \bar{f}(x) = 1$
6. Compute SVPSF matrix $L^{m(x)}$ using jump locations given by $J = \{x : |\bar{f}(x)| > \theta\}$
7. Restore signal $f_{m(x)}$ approximating f using $\text{diag}(C_{m(x)})L^{m(x)}$ for L in (2.5)

3.3. Numerical Results. Table 3.1 shows relative l^2 errors for restorations of the test function in Figure 2.1 with stencils up to order $m = 5$. The standard FOTV restoration is compared to two VOTV restorations, one using the **estimated** jump locations in Algorithm 2 (VOTV1) and one using the **true** jump locations (VOTV2). Results for different blurs and parameter choices λ are reported. The FOTV restoration is computed by solving (2.1), the VOTV1 restoration is computed using Algorithm 2, and the VOTV2 restoration by solving (2.5) where $L^{m(x)}$ is constructed using the true jump locations and $\sigma = \mathbf{Fid}_h(\mathbf{f}_1, g)$, i.e. the residual of the FOTV restoration.

In most cases our method results in a smaller relative l^2 error than the FOTV restoration for the same residual σ . In cases where the error in VOTV2 is smaller than in VOTV1, jump locations are either under or over estimated, i.e. either false jump discontinuities are identified or true jump discontinuities are missed. Figure 3.3 shows case 6 in Table 3.1 in which VOTV1 misses the fourth jump resulting in some oscillations around the fourth jump. Case 4 demonstrates that all jump discontinuities are eventually identified as the FWHM is reduced and less blurring is introduced into the problem. The same results hold for smaller values of λ , see cases 1-3 and for higher resolutions, see cases 10-15. In addition to the lower l^2 error, the VOTV restoration also represents the smooth regions of the signal much better than FOTV in Figure 2.1. This is confirmed in Figure 3.3 which shows that the pointwise errors are reduced. Figure 3.3 also demonstrates that the sizes and locations of the jump discontinuities are preserved by the method in Algorithm 2.

Cases 7-9 demonstrate the case of out of focus blur⁵. All jump discontinuities are identified correctly and the VOTV1 and VOTV2 restorations are identical. As in cases 1-6 the relative l^2 error is smaller in the VOTV case and the smooth regions are better represented than in the FOTV restoration as illustrated in Figure 3.4.

4. Conclusions. We have presented a new method to adaptively choose the local orders of a VOTV regularization of piecewise smooth functions. The method combines edge detection using local difference operators and HOTV regularization. As compared to the use of the traditional FOTV regularization, our variable order linear regularization operator better restores piecewise smooth functions that are blurred by either Gaussian or out of focus PSFs of varying widths. Concurrently, an approximation of the jump function which reveals the locations of the jump discontinuities in the underlying true signal is obtained. Numerical

⁵An out of focus blur may result in a two dimensional applications from a camera system that is out of focus. The corresponding PSF is constant on a disk and the one dimensional case is illustrated in Figure 3.4(a)

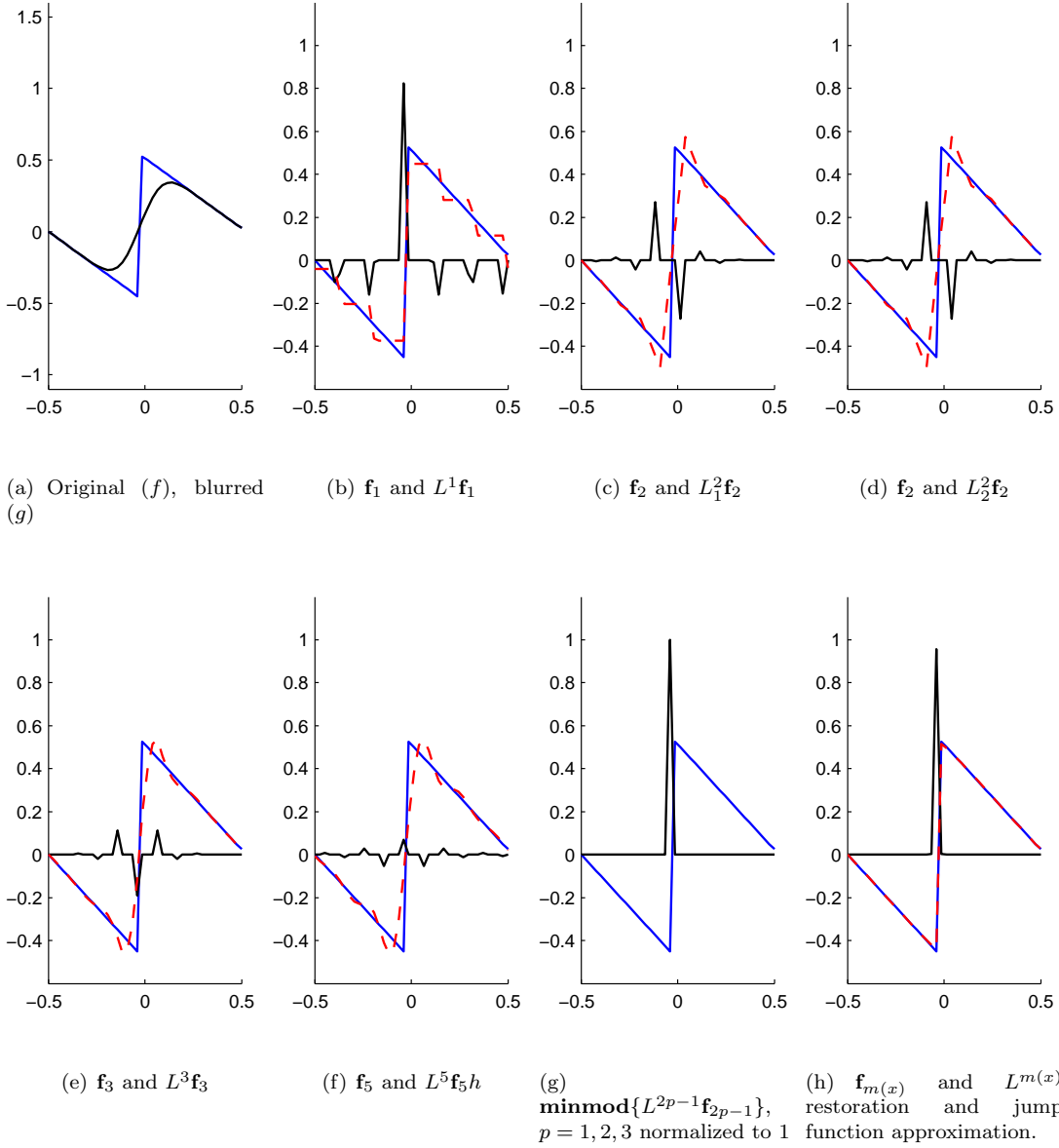


FIG. 3.2. Example HOTV regularization of the deconvolution problem. In each case the light (blue online) line is the true function f , the dashed (red online) line the signal restoration \mathbf{f}_m and the dark line is $L_i^m\mathbf{f}_m$, except in (a) where the dark is the blurred signal g and (g) where the dark is the *minmod*. The solution is piecewise constant for $m = 1$, piecewise linear for $m = 2$, piecewise quadratic for $m = 3$, etc. Panels (c) and (d) demonstrate that the even order derivatives should not be used in the deconvolution. We use an order dependent scaling in Algorithm 2 to compensate for the decreasing size of $L_i^m\mathbf{f}_m$ illustrated in the figure.

results show that such high order methods are particularly useful in cases where only limited resolution is available for the restoration of small features in the signal.

The method, based on FOTV, replaces the linear first order difference operator used in FOTV by a variable order difference operator with increasing order away from jump discontinuity locations. We use the contact point locations of polynomial segments from HOTV regularized restorations to estimate the jump discontinuity locations from the blurred data. All stages in the procedure can be posed as SOCPs and can, therefore, be solved using standard SOCP solvers.

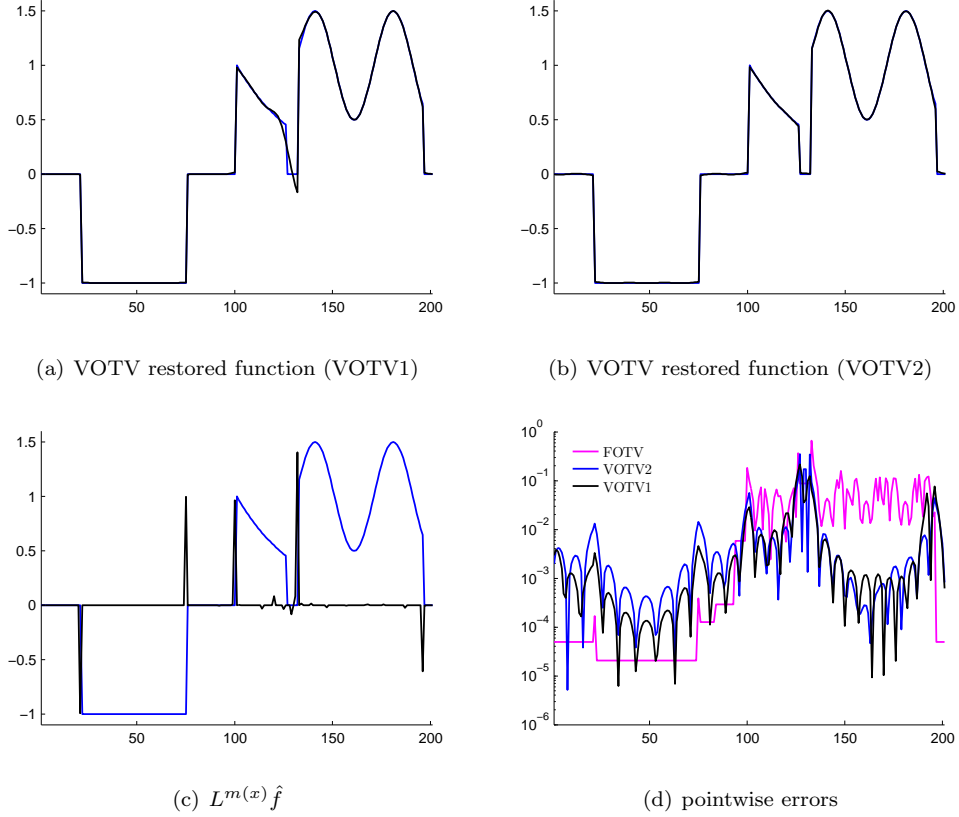


FIG. 3.3. Case 6 in Table 3.1: Restoration of the blurred test function in Figure 2.1 using Algorithm 2 with an l^2 error of .033 (a) and VOTV regularization with $L^m(x)$ obtained from the true jump locations with an l^2 error of .0069 (b). Panel (c) shows the jump function approximation obtained from the VOTV restoration (VOTV1) and panel (d) the pointwise errors in the FOTV as compared to the errors in VOTV1 and VOTV2.

Nr.	PSF	N	λ	FWHM	FOTV	VOTV1 minmod	VOTV2 true jump function
1	h_1	201	1.0e-05	3	0.00290	0.00011	0.00011
2	h_1	201	1.0e-05	5	0.02500	0.02105	0.00059
3	h_1	201	1.0e-05	9	0.04566	0.02332	0.00265
4	h_1	201	1.0e-03	3	0.00849	0.00096	0.00095
5	h_1	201	1.0e-03	5	0.03457	0.02509	0.00319
6	h_1	201	1.0e-03	9	0.08301	0.03335	0.00687
7	h_2	201	1.0e-05	12	0.00105	0.00028	0.00028
8	h_2	201	1.0e-03	12	0.01292	0.00557	0.00557
9	h_2	201	1.0e-02	12	0.03418	0.02744	0.02258
10	h_1	401	1.0e-05	5	0.01290	0.00016	0.00012
11	h_1	401	1.0e-05	11	0.03087	0.00639	0.00144
12	h_1	401	1.0e-05	17	0.05707	0.03026	0.04823
13	h_1	401	1.0e-03	5	0.01462	0.00374	0.00086
14	h_1	401	1.0e-03	11	0.04234	0.05316	0.01978
15	h_1	401	1.0e-03	17	0.09161	0.09419	0.10478
16	h_2	401	1.0e-05	25	0.00135	0.00038	0.00038
17	h_2	401	1.0e-03	25	0.01028	0.00507	0.00507
18	h_2	401	1.0e-02	25	0.03384	0.03579	0.02401

TABLE 3.1

Relative l^2 errors of the VOTV restoration with jump locations estimated from the *minmod* procedure described in Algorithm 2, in comparison to VOTV using the true locations of the jump discontinuities and FOTV. The effect of different choices of PSFs, in particular a Gaussian (h_1) and out of focus (h_2), with different choices of FWHM is shown.

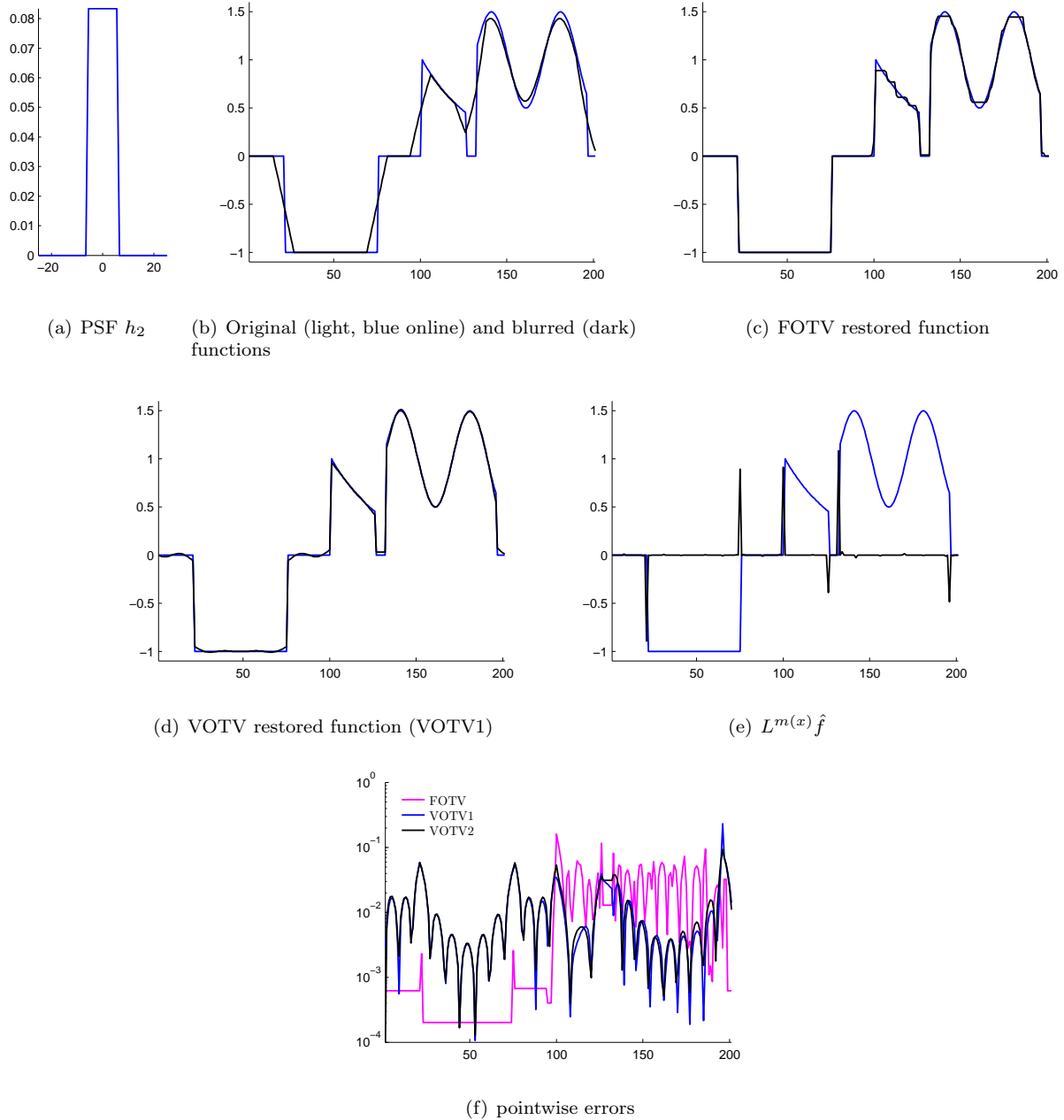


FIG. 3.4. Case 9 in Table 3.1: In (b) the piecewise smooth test function is contaminated by blurring with an out of focus PSF of 12 pixels width, illustrated in (a). Panel (c) shows the result of the FOTV restoration with $\lambda = 10^{-2}$, which yields an l^2 error of .034. Panel (d) shows the VOTV restoration with an l^2 error of .023. The estimation of the jump function is shown in panel (e) and the pointwise errors in panel (f).

Because the underlying edge detection method has also been very successfully applied to two dimensional signals, the logical next step is to extend the given method for two dimensional signal restoration. This could be of value when the method is used in applications such as restoring Positron Emission Tomography (PET) scans that are, after reconstruction from the collected data, blurry images with moderate to low resolution.

Acknowledgments. Rosemary Renaut has been supported in part by NSF grants DMS 0513214, DMS 0421846 and ITR 0324957.

Anne Gelb has been supported in part by NSF grants DMS 0510813, DMS 0513214 and ITR 0324957.

Appendix A. To gain understanding of the observation from the examples in Section 3 that the contact points of even order restorations can be used to identify jump discontinuities, we consider the approximation of a Heaviside step function with two polynomial segments of order N on the domain $[-1, 1]$ and one contact point at $x = \xi \in [0, 1)$,

$$p_1(x) = \sum_{k=0}^N a_k x^k, \quad p_2(x) = \sum_{k=0}^N b_k x^k.$$

For given ξ we seek to minimize

$$I(\xi) = \int_{-1}^0 (p_1(x))^2 dx + \int_0^{\xi} (p_1(x) - 1)^2 dx + \int_{\xi}^1 (p_2(x) - 1)^2 dx \quad (\text{A.1})$$

with respect to a_k and b_k , subject to the constraint conditions

$$p_1^{(p)}(\xi) = p_2^{(p)}(\xi) \quad \text{for } p = 0 \dots N - 1. \quad (\text{A.2})$$

We rewrite (A.1) and (A.2) in matrix-vector form,

$$\min_c I_N(\xi) = \frac{1}{2} c^T \Theta(\xi) c - \beta(\xi)^T c \quad \text{subject to} \quad \Upsilon(\xi) c = 0, \quad (\text{A.3})$$

where $c = [a \ b]^T \in \mathbb{R}^{2(N+1)}$, $\Theta(\xi) \in \mathbb{R}^{2(N+1) \times 2(N+1)}$, $\beta(\xi) \in \mathbb{R}^{2(N+1)}$ and $\Upsilon(\xi) \in \mathbb{R}^{N \times 2(N+1)}$, and are given by

$$\Theta(\xi) = \left(\begin{array}{c|c} \Theta_a(\xi) & 0 \\ \hline 0 & \Theta_b(\xi) \end{array} \right), \quad \beta(\xi) = \left(\begin{array}{c} \beta_a(\xi) \\ \beta_b(\xi) \end{array} \right), \quad \Upsilon(\xi) = (\Upsilon_a(\xi) \mid -\Upsilon_a(\xi))$$

with

$$\begin{aligned} \Theta_a(\xi)_{i_1, j} &= \frac{\xi^{i_1+j-1} - (-1)^{i_1+j-1}}{i_1+j-1} & \Theta_b(\xi)_{i_1, j} &= \frac{1 - \xi^{i_1+j-1}}{i_1+j-1} \\ \beta_a(\xi)_{i_1} &= \frac{\xi_1^{i_1}}{i_1} & \beta_b(\xi)_{i_1} &= \frac{1 - \xi_1^{i_1}}{i_1} \\ \Upsilon_a(\xi)_{i_2, j} &= \begin{cases} \frac{(j-1)!}{(j-i_2)!} \xi^{j-i_2} & \text{if } i_2 \leq j \\ 0 & \text{otherwise} \end{cases} \end{aligned}$$

where $0! = 1$, $\xi^0 = 1$, $i_1, j = 1, \dots, N+1$ and $i_2 = 1, \dots, N$. Using Lagrange multipliers, collected in $\Lambda \in \mathbb{R}^N$, the solution of (A.3) can be found by obtaining the solution of the linear system of equations

$$\left(\begin{array}{cc} \Theta(\xi) & \Upsilon(\xi)^T \\ \Upsilon(\xi) & 0 \end{array} \right) \left(\begin{array}{c} c \\ \Lambda \end{array} \right) = \left(\begin{array}{c} \beta(\xi) \\ 0 \end{array} \right). \quad (\text{A.4})$$

The coefficient vector c is explicitly given using the block matrix formulation (A.4) as

$$c(\xi) = (\Theta^{-1}(\xi) + \Theta^{-1}(\xi) \Upsilon(\xi)^T S_a^{-1} \Upsilon(\xi) \Theta^{-1}(\xi)) \beta(\xi), \quad (\text{A.5})$$

where $S_a := -\Upsilon(\xi) \Theta^{-1}(\xi) \Upsilon(\xi)^T$ is the Schur complement of $\Theta(\xi)$, see [10, 6]. The inverses of $\Theta(\xi)$ and $S_a(\xi)$ can be computed using Gauss elimination, resulting in a rational function $I_N(\xi)$ in (A.3), e.g. for $N = 1$

$$I_1(\xi) = -\frac{7 + 21\xi + 24\xi^2 + 4\xi^3}{16(1 + \xi)^3},$$

which has a minimum at $\xi = 1/2$. In other words the contact point between the line segments has to be placed at $\xi = 1/2$ to minimize the \mathcal{L}^2 -fit of two line segments with continuous contact condition. In particular the location of the contact point cannot be used to determine the location of the jump in the original step function.

A necessary condition for $\xi = 0$ being the best contact point is, obviously, that $I_N(\xi)$ is increasing at $\xi = 0$. We therefore consider the Taylor expansions of $I_N(\xi)$ for different N :

- $N = 1$:

$$I_1(\xi) = -\frac{7}{16} - \frac{3\xi^2}{16} + O(\xi)^3$$

- $N = 2$:

$$I_2(\xi) = -\frac{17}{36} + \frac{35\xi^2}{144} + O(\xi)^3$$

- $N = 3$:

$$I_3(\xi) = -\frac{119}{256} - \frac{7\xi^2}{256} + O(\xi)^3$$

- $N = 4$:

$$I_4(\xi) = -\frac{191}{400} + \frac{351\xi^2}{6400} + O(\xi)^3$$

To second order, I_2 and I_4 are minimum at $\xi = 0$, while I_1 and I_3 are not. The presented analysis provides some support for the following claims:

1. For even order approximations the smallest error is obtained by choosing $\xi = 0$.
2. For odd order approximations the smallest error is obtained by choosing $\xi > 0$.
3. Together these results support our use in Section 3 of only the odd polynomials for the identification of the locations of the jump discontinuities from the contact points of the polynomial segments.

There is clearly the need for a more elaborate analysis of this subject. This is, however, beyond the scope of this experimental paper.

Appendix B.

- FD** Finite Difference
- FOTV** First Order Total Variation
- FWHM** Full Width at Half Maximum
- HOTV** Higher Order Total Variation
- LS** Least Squares
- PET** Positron Emission Tomography
- PDE** Partial Differential Equation
- PSF** Point Spread Function
- KKT** Karush-Kuhn-Tucker
- SIPSF** Spatially Invariant Point Spread Function
- SOCP** Second Order Cone Program
- SVPSF** Spatially Variant Point Spread Function
- TV** Total Variation
- VOTV** Variable Order Total Variation
- VOTV1** VOTV with estimated jump positions
- VOTV2** VOTV with true jump positions

REFERENCES

- [1] R. Archibald, A. Gelb, and J. Yoon. Polynomial Fitting for Edge Detection in Irregularly Sampled Signals and Images. *SIAM Journal on Numerical Analysis*, 43(1):259–279, 2005.

- [2] R. Archibald, A. Gelb, and J. Yoon. Determining the locations and discontinuities in the derivatives of functions. *Applied Numerical Mathematics*, 58(5):577–592, May 2008.
- [3] E. Candes, J. Romberg, and T. Tao. Robust uncertainty principles: Exact signal reconstruction from highly incomplete frequency information. *IEEE Transactions on Information Theory*, 52(2):489–509, February 2006.
- [4] E. Candes and T. Tao. Near-Optimal Signal Recovery From Random Projections: Universal Encoding Strategies? *IEEE Transactions on Information Theory*, 52(12):5406–5425, December 2006.
- [5] J. F. Claerbout and F. Muir. Robust modeling with erratic data. *Geophysics*, 38(5):820–844, October 1973.
- [6] J. Demmel. *Applied Numerical Linear Algebra*. SIAM, Philadelphia, 1997.
- [7] B. Fornberg. Generalization of Finite Difference Formulas on Arbitrarily Spaced Grids. *Mathematics of computation*, 51(184):699–706, October 1988.
- [8] A. Gelb and E. Tadmor. Adaptive Edge Detectors for Piecewise Smooth Data Based on the minmod Limiter. *Journal of Scientific Computing*, 28(2-3):279–306, September 2006.
- [9] D. Geman. Constrained Restoration and the Recovery of discontinuities. *IEEE Transactions on Pattern Analysis and Machine Intelligence*, 14(3):367–383, March 1992.
- [10] G. H. Golub and C. van Loan. *Matrix Computations*. John Hopkins Press, Baltimore, second edition, 1989.
- [11] M. Grant, S. Boyd, and Y. Ye. *Disciplined Convex Programming*, pages 155–210. Nonconvex Optimization and its Applications. Springer, 2006.
- [12] M. Grant, S. Boyd, and Y. Ye. CVX: Matlab Software for Disciplined Convex Programming, September 2007.
- [13] P. C. Hansen. *Rank-Deficient and Discrete Ill-Posed Problems: numerical aspects of linear inversion*. Society for Industrial and Applied Mathematics, Philadelphia, PA, USA, 1998.
- [14] R. J. LeVeque. *Finite Volume Methods for Hyperbolic Problems*. Cambridge Texts in Applied Mathematics (No. 31). Cambridge University Texts, Cambridge, UK, 2002.
- [15] Y. Lin and B. Wohlberg. Application of the UPRE Method to Optimal Parameter Selection for Large Scale Regularization Problems. *2008 IEEE Southwest Symposium on Image Analysis and Interpretation*, March 2008.
- [16] J. Mead and R. A. Renaut. The χ^2 -curve method of parameter estimation for generalized Tikhonov regularization. *submitted to Inverse Problems*, August 2008.
- [17] J. Nocedal and S. J. Wright. *Numerical Optimization*. Springer-Verlag, New York, 1999.
- [18] L. I. Rudin, S. Osher, and E. Fatemi. Nonlinear total variation based noise removal algorithms. *Physica D*, 60:259–268, 1992.
- [19] R. Saxena, A. Gelb, and H. D. Mittelmann. A High Order Method for Determining the Edges in the Gradient of a Function. *Global Science*, Preprint, 2007.
- [20] V. Solo. Selection of Regularisation Parameters for Total Variation Denoising. In *IEEE International Conference on Acoustics, Speech, and Signal Processing*, volume 3, pages 1653–1655, March 1999.
- [21] D. M. Strong and T. F. Chan. Relation of Regularization Parameter and Scale in Total Variation Based Image Denoising. Technical report, UCLA Department of Mathematics, June 1996.
- [22] D. M. Strong and T. F. Chan. Edge-Preserving and Scale Dependent Properties of Total Variation Regularization. *Report 9848, Department of Mathematics, UCLA*, page <http://www.math.ucla.edu/applied/cam/index.html>, 2000.
- [23] J.F. Sturm. Using SeDuMi 1.02, a MATLAB toolbox for optimization over symmetric cones. *Optimization Methods and Software*, 11–12:625–653, 1999. Special issue on Interior Point Methods (CD supplement with software), <http://sedumi.mcmaster.ca/>.
- [24] K. Toh, R. Tütüncü, and M. Todd. SDPT3 4.0 (beta) (software package). Technical report, Department of Mathematics National University of Singapore, September 2006. <http://www.math.nus.edu.sg/~mattohkc/sdpt3.html>.
- [25] C. R. Vogel. *Computational Methods for Inverse Problems*. Society for Industrial and Applied Mathematics, Philadelphia, PA, USA, 2002.
- [26] Y. Wang, W. Yin, and Y. Zhang. A Fast Algorithm For Image Deblurring with Total Variation Regularization. Technical Report CAAM TR07-10, Department of Computational and Applied Mathematics, Rice University, Houston, Texas 77005, June 2007.